Eur. Phys. J. D **13**, 337–344 (2001)

THE EUROPEAN PHYSICAL JOURNAL D

EDP Sciences

Semi-classical analysis of helium broadened acetylene ($\nu_1 + 3\nu_3$) band transitions measured by a NIR diode laser spectrometer

B.K. Dutta, D. Biswas, B. Ray, and P.N. Ghosh[a]

Department of Physics, University of Calcutta, 92 A.P.C. Road, Calcutta – 700 009, India

Received 27 July 2000 and Received in final form 15 November 2000

Abstract. Helium-broadened line shapes of the rovibrational transitions of the ($\nu_1 + 3\nu_3$) combination-overtone band of C_2H_2 have been studied by using a near IR diode laser spectrometer. The $2f$ frequency detection technique has been employed for signal detection of these weak band transitions. The linestrength parameters and broadening coefficients (HWHM) have been extracted by fitting the observed line shapes with Voigt profiles. Helium, lightest noble gas perturber, exhibits the effect of close collisional dephasing on pressure broadened line profiles. Due to overlapping of atomic orbitals the repulsive interaction dominates over attractive interaction for collision diameter in the 3 to 4 Å range. In order to interpret this type of linear polyatomic–monatomic collision phenomena the Tipping–Herman potential has been chosen. Emphasis has been given to the analysis of observed data to obtain information about interaction potential, phase-shift and molecular constants. The results obtained from detailed semi-classical model calculations are found to be in good agreement with the observed data.

PACS. 42.62.Fi Laser spectroscopy – 33.70.-w Intensities and shapes of molecular spectral lines and bands – 33.70.Jg Line and band widths, shapes, and shifts

1 Introduction

The high resolution near infrared spectroscopic measurement of collision broadened line profiles of overtone band transitions of acetylene, a trace component in the earth atmosphere, is important as far as atmospheric monitoring and pollution control measurements are concerned. The ($\nu_1 + 3\nu_3$) band transitions of acetylene were studied earlier [1–5] by employing several spectroscopic methods. Six rovibrational components (P7, P8, P13, P15, R9 and R11) of the ($\nu_1 + 3\nu_3$) band of C_2H_2 around 788 nm, were observed by using a high resolution diode laser spectrometer to measure the pressure broadened linewidth and intensity in the self- and N_2-perturbed cases [6]. In a recent paper we have reported O_2- and air-broadening coefficients and linestrength parameters for these same transitions of the ($\nu_1 + 3\nu_3$) band of C_2H_2 [7]. Measurements of helium broadened line shapes and their theoretical analyses reported in this work are a continuation of our previous work for the same transitions. Recently, line broadening measurements of the vibrational bands of several atmospheric molecules in the presence of helium were made [8–12]. Measurements in the presence of other inert gases were also reported [13,14].

In the theory of molecular collisions, the broadening caused by inert gases has always attracted special attention. Inert gases possess closed electron shells and they do not have permanent electrical moments in the electronic ground state. They may be considered as structureless particles owing to the fact that the energy required to excite them is greater than the mean thermal energy. Experimental and theoretical investigations of molecular absorption profile induced by collisions with atoms or molecules are interesting for the analysis of intermolecular forces. The observed broadening parameters allow us to estimate the parameters of the intermolecular interaction potential, collision cross-section relating to collision diameter, the polarizability of the absorbing molecules and so on. Theoretical calculations of pressure broadening coefficients are carried out on the basis of semi-classical line broadening theory, developed by Anderson [15] and later suitably modified by Tsao and Curnutte [16]. The classical limit in trajectory for collision between absorber and perturber is estimated from the isotropic part of the Tipping–Herman (TH) potential. It may be noted that the contributions of vibrational effect should be small in this case of weak fourth order combination-overtone band and hence, have been neglected in the calculation. In order to circumvent the problem of a sharp cutoff of the impact parameter in the halfwidth calculation proposed in Anderson-Tsao-Curnatte (ATC) model, the calculation is also attempted in the Robert-Bonamy (RB) model [17] using classical path assumption and the calculated values

[a] e-mail: png@cubmb.ernet.in

are compared with the observed values. We also report the impact parameter dependence of phase-shift and the relative contribution of the repulsive and attractive parts of the TH-potential in the phase-shift.

2 Experimental

The spectra were recorded by using a commercial GaAlAs diode laser (Hitachi HL7838G), having a standard wavelength range 770–790 nm with a typical value of 780 nm and an emission power of 20 mW. The limiting drive current for this diode is 70 mA and the temperature range used for wavelength scanning is 26–50 °C. The diode laser is driven by a low noise current source with a wavenumber dependence of 0.1 cm^{-1}/mA and a temperature controller with temperature tunability at 0.084 nm/°C. The long term stability of the temperature controller is better than 10 mK at any operating temperature, leading to a wavenumber stability of better than 0.01 cm^{-1} for a measurement of frequency carried out for a long time. The short term ripples of the diode are of the order of 10 MHz in the free running mode for a period of a few seconds. The measurement of one particular transition covering nearly 10 GHz takes nearly 5 seconds. So, the measurement precision is better than 0.003 cm^{-1}. The long term drift of the current is less than 10 ppm, this leads to negligible fluctuation of laser frequency. The experimental setup is the same as discussed in reference [11] and is not repeated in this paper. The sample was contained in a cylindrical glass cell of 1.5 m path length and 5 cm diameter. An Oriel monochromator is used for rough estimation of the wavelength region. The actual values of wavelength were taken from reference [1]. The simultaneous recording of etalon fringes (finesse = 36, FSR = 5.00 GHz) along with the absorption signal gives rise to the relative frequency calibration of the transitions. It also ensures the single mode nature of the laser frequency. For the in-phase detection a sinusoidal modulation at a frequency of 5 kHz with small modulation amplitude is applied to the diode laser injection current. The phase sensitive detection with the lock-in amplifier at a frequency of 10 kHz gives rise to the second derivative of the true absorption spectrum [6,7,18].

Commercial high purity (99+%) acetylene gas with natural isotopic abundance is used without further purification. Helium is procured from Aldrich and has a stated purity of 99.6+%. All the measurements are recorded at room temperature, (300 ± 1) K. The number of detectable lines in the measured spectral range of the diode laser is restricted due to the mode characteristic of the laser diode. Usually 2 to 4 transitions could be observed in one mode covering a range of nearly 7 cm^{-1}. For each of the spectral transitions, we have recorded He-broadened line shape in the pressure range 100 torr to 500 torr with a step size of 100 torr of the perturber keeping the absorber pressure fixed at 100 torr. MKS Baratron capacitance manometer, type 122B with a full scale of 1 000 torr, was used for pressure measurement. Measurement precision is 0.1 torr at pressures of the order of 100 torr.

3 Line shape analysis

For the simulation of spectral lines we have used Voigt profile which is the real part of the complex probability function and may be expressed as

$$\alpha_{\mathrm{V}}(\omega) = A\left(\frac{y}{\pi}\right) \int_{-\infty}^{+\infty} \frac{\exp\left(-\tau^2\right)}{y^2 + (x-\tau)^2}\, \mathrm{d}\tau. \qquad (1)$$

The dimensionless parameters x and y are defined as $x = (\omega - \omega_0)/\sigma$, $y = \Gamma/\sigma$. τ is the dimensionless parameter representing the Doppler shift normalized by the Doppler width and $A = \sqrt{\pi}\, S/\sigma$. Γ is the collisional half width arising from state (or phase) changing collisions. ω_0 is the line center frequency and $\sigma\,(= \omega_0\sqrt{2\,k_{\mathrm{B}}T/mc^2})$ is the calculated Doppler half width at e^{-1} intensity at temperature T. k_{B} is the Boltzmann constant and m is the molecular mass of the absorber. S is the linestrength parameter with the dimension of cm/molecule. The standard Voigt profile has been computed following the algorithm developed by Hui *et al.* [19]. The intensity $I\,(\omega)$ transmitted through the sample cell is given by Beer–Lambert's law

$$I(\omega) = I_0(\omega)\exp[-\alpha_{\mathrm{V}}(\omega)pl] \qquad (2)$$

where p is the absorber pressure, l is the sample path length and $I_0(\omega)$ is the intensity of the incoming radiation. It has been shown that $I_0(\omega)$ is almost constant for a frequency sweep of the order of several GHz. The transmittance is retrieved from the exponential part of equation (2). Here $\alpha_{\mathrm{V}}(\omega)pl$ is much less than a unit for all the transitions, the transmitted intensity $I(\omega)$ is proportional to $\alpha_{\mathrm{V}}(\omega)$. The recorded intensities are normalized with respect to the corresponding signals from the empty reference cell. Since the detection is performed at the second harmonic of the modulation frequency, the observed line profiles are strong second derivative spectra. The original dc absorption line shapes can be recovered by integrating the second derivative output. Here the derivative output is accurately determined for small modulation amplitude, ω_{m} [6]. To extract the line shape parameters the calculated transmission intensities are fitted with the observed profiles. A non-linear least squares fitting method based on Levenberg–Marquardt procedure [20,21] is used for extraction of line parameters. The Doppler HWHM $\sigma\sqrt{\ln 2}$ is kept constant at its theoretical value of 0.015 cm^{-1}, the pressure broadening coefficient Γ/P and the linestrength parameter S are chosen as floating parameters. A simulation of the true etalon fringes shows that the observed second derivative etalon fringes contain contributions from the laser linewidth, slow response from the detectors and other instrumental factors. A comparison of the observed etalon fringes with the simulated ones leads to a linewidth of 0.021 cm^{-1} arising from the above factors. Hence, a Lorentzian function having this width is convoluted with the calculated spectrum before fitting with the observed spectrum [6,7,12,18]. Figure 1 shows

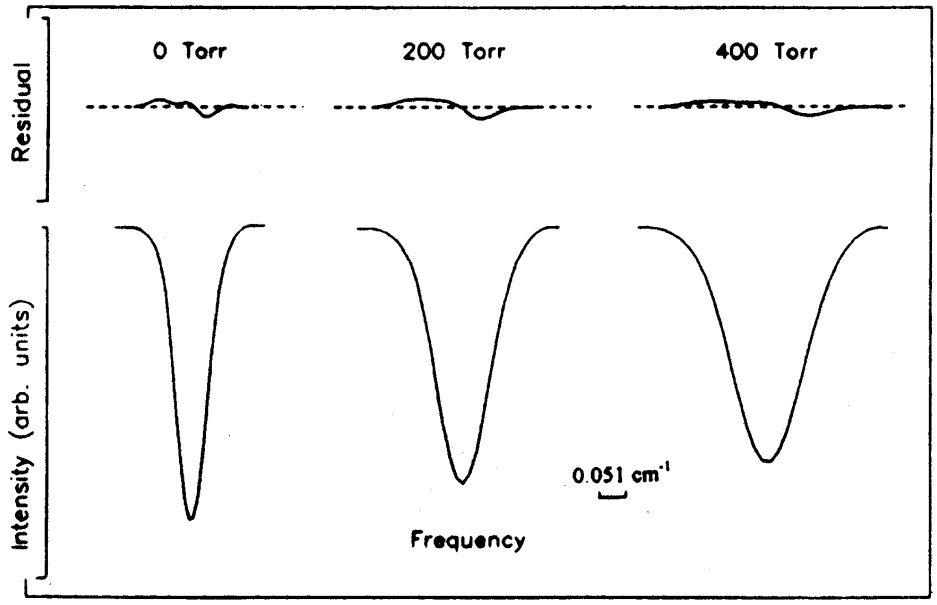

Fig. 1. Line shape of the C_2H_2 ($\nu_1 + 3\nu_3$) band transition P13 (12 641.15 cm^{-1}) for different He pressures (shown in the figure) for an absorber pressure of 100 torr. The upper traces plotted in the same scale as the observed line profile are the residuals of the observed and the least squares fitted Voigt profiles.

Table 1. Measured line strength values S (cm/molecule) and He-broadening coefficients Γ/P ($cm^{-1}atm^{-1}$) in the ($\nu_1 + 3\nu_3$) band of C_2H_2 with their calculated values.

Transition	ω_0^a (cm^{-1})	S (cm/molecule)	Γ/P ($cm^{-1}atm^{-1}$)		
			Obs.	Cal.	
				ATC	RB
P7	12 658.11	$2.597(15) \times 10^{-23}$	0.0491(1)	0.0505	0.0539
P8	12 655.37	$7.596(54) \times 10^{-24}$	0.0423(1)	0.0495	0.0538
P13	12 641.15	$4.758(19) \times 10^{-23}$	0.0477(5)	0.0438	0.0532
P15	12 635.18	$2.622(30) \times 10^{-23}$	0.0394(1)	0.0410	0.0529
R9	12 696.42	$6.307(21) \times 10^{-23}$	0.0622(1)	0.0475	0.0536
R11	12 699.91	$6.288(56) \times 10^{-23}$	0.0591(2)	0.0451	0.0534

[a] The line positions are taken from reference [1].
[b] The numbers in parentheses are one standard deviation, in units of least significant digits.

the observed He-broadened spectra retrieved from measured second derivative profiles after performing two successive numerical integrations for three different perturber pressures and a fixed absorber pressure. Here, the residuals represent the differences between the observed and the least squares fitted spectra. The residuals are somewhat large and asymmetric in nature. In the case of nitrogen broadened acetylene infrared band transitions, Bouanich *et al.* [22] found very large residuals by fitting with the Voigt profiles. The residuals were reduced by fitting with the Rautian profiles which included narrowing effect. In our case, we attempted fitting with a collisionaly narrowed Galatry profile [23] without any improvement. In fact no improvement is expected in this case because of the inherent symmetry of the Voigt profiles, since the shape of the residuals reveals the asymmetric nature of the line shape. It may be mentioned here that the gas pressure used in all the measurement for the near infrared band is much larger than the pressure used in the infrared region. The observed asymmetry may be induced by the relatively large pressure of both the absorber and perturber molecules. This kind of asymmetry was found consistently in the case of all the transitions measured in this region. Small effect of pressure induced asymmetry was also found in the case of Ar-broadened HF infrared transitions [24]. In this case the residuals were considerably reduced when Voigt profiles were replaced by Rautian or Galatry line shape functions, thus indicating the presence of narrowing induced by velocity changing collisions. For interpretation of line shape asymmetry they [24] used correlation between velocity and phase changing collisions. In our case, since the use of Galatry profiles could not improve the residuals there is no possibility of using any such correlation term. Also, the correlation parameters used in [24] were empirical in nature and had no direct physical interpretation. As emphasized by Pine [24], line shape asymmetries may also arise from several other factors. In our case the laser line shape may have small asymmetry that has not been taken into consideration in the Lorentzian function, that was convoluted with the calculated spectrum before fitting as mentioned earlier. The nonlinear nature of wavenumber scan may also be responsible for the asymmetry.

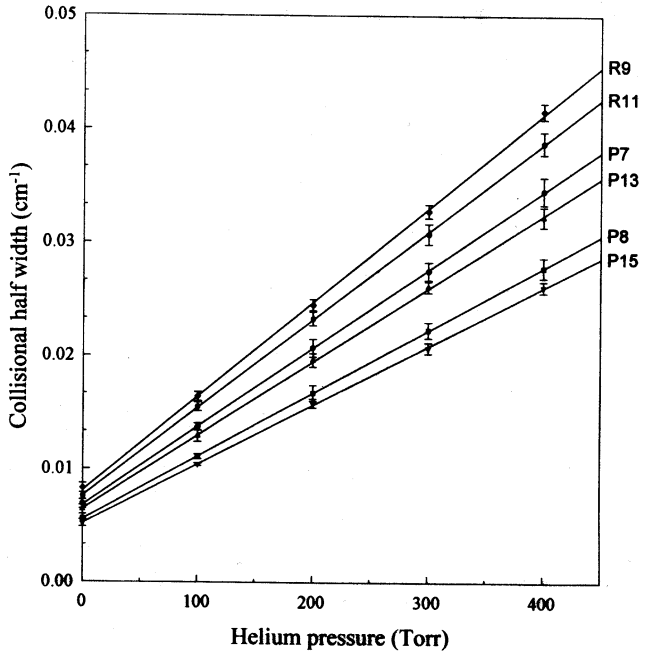

Fig. 2. Collisional half widths of the C_2H_2 ($\nu_1 + 3\nu_3$) band transitions in the presence of He perturber derived from the least squares fitted Voigt profiles. The vertical bars represent the standard errors obtained from the computer fitting.

These factors are beyond the scope of our quantitative analysis. It may be mentioned here that the effect of asymmetry in the wings of line profiles is significant for accurate determination of the values of line shift, but they are not expected to affect the values of line broadening parameters, Γ. For the four P-branch and two R-branch transitions the measurement and fitting processes are carried out for five different pressures of the perturber. The values of the broadening parameter, Γ increase linearly when increasing the perturber pressure (Fig. 2). The vertical error bars in Figure 2 represent the standard errors obtained from computer fitting of the spectral data. The magnitude of the error bar is found to be of the order of 6% of the collisional halfwidth values for the P-branch transitions and 4% for the R-branch transition at zero pressure of He. This error-contribution will be decreased by 3% for higher He pressure up to 400 torr for both the transitions. These errors are used in the linear fit of data at different pressures to compute mean Γ/P and S (Tab. 1) values. The observed values of Γ/P show a slow decrease with increasing value of the quantum number J for the P-branch transitions in the range of J-values investigated. If we compare the S values for self, nitrogen, oxygen and air perturber cases [6,7] with the helium broadened case, it is found that the S values show variation with change of collision partners and this variation depends on the transitions. The different types of collision partners at high pressure may cause a small shift of the baselines. This may lead to a variation in linestrength parameters obtained by fitting. It may be noted that mean values of S for He broadening cases are comparable with those for the self, nitrogen, oxygen and air perturber cases [6,7].

4 Theoretical analysis

The pressure broadening coefficients of the absorption lines of acetylene perturbed by rare helium gas are calculated on the basis of semi-classical impact theory [16,17], under stationary path assumption. The interaction potential considered in our case is the TH-potential [25]. The interaction of a linearly symmetric acetylene molecule with a helium atom takes the form [22],

$$V_{\mathrm{TH}} = 4\epsilon\left[\left(\frac{\sigma}{r}\right)^{12} - \left(\frac{\sigma}{r}\right)^{6}\right] + 4\epsilon\left[R_2\left(\frac{\sigma}{r}\right)^{12} - A_2\left(\frac{\sigma}{r}\right)^{6}\right] P_2(\cos\theta). \quad (3)$$

The short range repulsive interaction is important to take into account the effect of close collisions and is expressed by the r^{-12}-order terms in the potential. The r^{-6}-order terms include the effect of long range dispersive interaction. The second part of the potential includes the orientation effect of the active molecule during collision, introducing anisotropy in polarizability (γ). Here, $R_2 = A_2 = \gamma = (\alpha_\parallel - \alpha_\perp)/(\alpha_\parallel + 2\alpha_\perp)$. $\alpha_\parallel$ and $\alpha_\perp$ are the parallel and perpendicular components of the polarizability of acetylene, r is the intermolecular distance of the colliding partners and θ is the angle between the axis of the active molecule and the intermolecular axis. The parameters ϵ and σ measure the strength of the attraction and the radius of the repulsive core respectively. For the molecular pair C_2H_2–He, ϵ and σ are usually determined by Lorentz–Berthelot's rule, $\epsilon = \sqrt{\epsilon_1\epsilon_2}$ and $\sigma = (\sigma_1 + \sigma_2)/2$, where ϵ and σ are the Lennard–Jones (L–J) parameters having subscripts 1 and 2 for acetylene and helium respectively. However, this rule may have some finite chance of overestimation of the well depth. For this reason, we follow the combination rule proposed by Sikora [26]

$$\epsilon = (\epsilon_1\epsilon_2)^{\frac{1}{2}} f_1(U) f_2(V) \quad (4)$$

$$f_1(U) = \frac{4U}{(1+U)^2}; \qquad U = \frac{U_2}{U_1}$$

$$f_2(V) = \frac{2^{13}\, V^{\frac{1}{2}}}{(1+V^{\frac{1}{13}})^{13}}; \qquad V = \frac{\epsilon_2\,\sigma_2^{12}}{\epsilon_1\,\sigma_1^{12}}$$

$$\sigma = 2^{-\frac{13}{12}}\left(\sigma_1^{\frac{12}{13}} + \sigma_2^{\frac{12}{13}}\right)^{\frac{13}{12}}. \quad (5)$$

Here $U_{1,2}$ denotes the ionization potential.

Since the perturber is spherical it has no rotational transitions. If $F(v)$ is the Maxwell–Boltzmann velocity distribution function for relative velocity of approach, v of two colliders, $S(b,v)$ is the probability of collision induced transitions of the active molecule over the rotational states for a certain impact parameter b; and the expression for pressure broadened half width ($\mathrm{cm}^{-1}\mathrm{atm}^{-1}$) of a single absorption line can be written in general,

$$\Gamma_{\mathrm{c}} = \frac{N}{2\pi c}\int_0^\infty F(v)\,\mathrm{d}v \int_0^\infty S(b,v)\,2\pi b\,\mathrm{d}b \quad (6)$$

where,

N = number of colliding molecules per atmospheric pressure,
c = velocity of light,
b = impact parameter.

Under ATC formalism, valid for uniform collisional velocity, we take the mean collisional velocity, $\bar{v} = \sqrt{8k_{\rm B}T/m\pi}$, where T is the ambient temperature and m is the reduced mass of the molecular pair. For a second order perturbation term of the collisional Hamiltonian involved in line broadening theory, we require only the $S_2(b,\bar{v})$ term [16]. By imposing the condition of the straight line trajectory model, the probability function retrieved from reference [17] is given in the following form,

$$S_2(b,\bar{v}) = \left[\frac{4\epsilon\sigma}{\hbar\,\bar{v}}\right]^2 \left[\frac{21\pi^2}{2\,560}\,A_2^2\,\left(\frac{\sigma}{b}\right)^{10} M_{10}(k) - \frac{63\pi^2}{5\,120}\,A_2R_2\,\left(\frac{\sigma}{b}\right)^{16} M_{16}(k) + \frac{48\,951\pi^2}{10\,485\,760}\,R_2^2\,\left(\frac{\sigma}{b}\right)^{22} M_{22}(k)\right]. \quad (7)$$

Here,

$$M_{10}(k) = \sum_{J_{\rm i}'} C^{(2)}_{J_{\rm i}'}\,f_{10}(k) + \sum_{J_{\rm f}'} C^{(2)}_{J_{\rm f}'}\,f_{10}(k) + D$$

$$M_{16}(k) = \sum_{J_{\rm i}'} C^{(2)}_{J_{\rm i}'}\,f_{16}(k) + \sum_{J_{\rm f}'} C^{(2)}_{J_{\rm f}'}\,f_{16}(k) + D$$

$$M_{22}(k) = \sum_{J_{\rm i}'} C^{(2)}_{J_{\rm i}'}\,f_{22}(k) + \sum_{J_{\rm f}'} C^{(2)}_{J_{\rm f}'}\,f_{22}(k) + D \qquad \text{and}$$

$$D = (-1)^{(J_{\rm i}+J_{\rm f})}\,2\,\left[(2J_{\rm i}+1)(2J_{\rm f}+1)\,C^{(2)}_{J_{\rm i}'}\,C^{(2)}_{J_{\rm f}'}\right]^{\frac{1}{2}} \times W(J_{\rm i}\,J_{\rm f}\,J_{\rm i}\,J_{\rm f}\,;\,12)$$

$J_{\rm i}'$ and $J_{\rm f}'$ denote the collision perturbed states. W is the Racah-coefficient [16]. All the C_J's are the Clebsch-Gordon coefficients which actually define the transition probability of the active molecule in the collision perturbed J-states following the selection rule $\Delta J = 0, \pm 2$. In general, $C^{(2)}_{J'} = |\langle J200|J'0\rangle|^2$. This can be calculated as stated in reference [27]. $f_{10}(k)$, $f_{16}(k)$ and $f_{22}(k)$ are the normalized off-resonance functions retrieved from ${}^{2,0}f_6^6(k)$, ${}^{2,0}f_6^{12}(k)$ and ${}^{2,0}f_{12}^{12}(k)$ respectively, given in reference [17]. By considering the classical path assumption introduced into the ATC model, the off-resonance parameter can be written as,

$$k = \frac{2\pi c}{\bar{v}}\,b\,\Delta E \quad (8)$$

where, ΔE, the off-resonance energy, depends on the rotational constants $B_{\rm i}$ and $B_{\rm f}$ of the initial and final states respectively of the active molecule for the transition. The nearest possible distance of approach d, of the colliding molecules for unavoidable cutoff proposed by Anderson, is calculated by using the isotropic part of the TH-potential as stated in references [28,29]. This well defined parameter in the combined potential configuration can remove the problem of the overestimation of the effect of close collisional interaction. We get,

$$\int_0^\infty S(b,\bar{v})\,2\pi b\,{\rm d}b = \pi\,d^2\,S_2(d,\bar{v}) + \int_d^\infty S_2(b,\bar{v})\,2\pi b\,{\rm d}b. \quad (9)$$

Here, $S_2(d,\bar{v})$ limits the collision probability of the active molecule for specific rotational states. The integration over b is performed by a simple computer program which increases b with a step size of 0.001 Å till convergence is achieved. From the calculations carried out, for two stated combination rules from lower J to higher J (up to 35) of the absorber, we conclude that the J-dependence of $\Gamma_{\rm c}$ is somewhat better for Sikora's combination rule to calculate the potential parameters (Tab. 2). The anisotropy in polarizability, γ, calculated from $\alpha_\parallel$ and $\alpha_\perp$, is 0.30. The half widths ($\rm cm^{-1}atm^{-1}$), calculated using this γ value and other parameters, deviate nearly 43–48% from their experimentally measured values. It needs some adjustment of parameters. If the values of ϵ and σ are arbitrarily changed, the isotropic potential configuration will be changed for their different sets of values. As the contribution from the vibrational dephasing effect for this part of the potential has been neglected in our calculation for the weak combination-overtone band transition, we take a fixed set of source values for ϵ and σ. The value of γ will include the effect of long range dispersion interaction, due to the relative orientation of the colliding molecules as well as their charge density fluctuation over the small collision interval, which varies with the strength of collision for different rovibrational bands. However, the spectroscopic source value of γ is not available in our case. We had a similar problem of non-availability of γ values which was also noted in reference [22]. By adjusting the value of γ, we obtained (for $\gamma = 0.40$) a good agreement between experimental and calculated values (Tab. 1). The pressure broadening coefficients, calculated with the ATC model, show a dressing trend (Fig. 3) with increasing

Table 2. Molecular parameters used in the calculations.

Parameters	C_2H_2	He
$U\times10^{11}$ (erg)	1.14 [a]	3.915 [b]
$\alpha_\parallel \times 10^{25}$ (e.s.u.) [c]	51.2	–
$\alpha_\perp \times 10^{25}$ (e.s.u) [c]	24.3	–
B_0 ($\rm cm^{-1}$) [d]	1.17692	–
B_v ($\rm cm^{-1}$) [e]	1.15096	–
ϵ (K)	199.2 [f]	10.3 [g]
σ (Å)	4.523 [f]	2.609 [g]
γ ⋆	0.40	–

⋆ Adjusted value (see text); [a] reference [30], [b] reference [28], [c] reference [31], [d] reference [32], [e] reference [4], [f] reference [33], [g] reference [34].

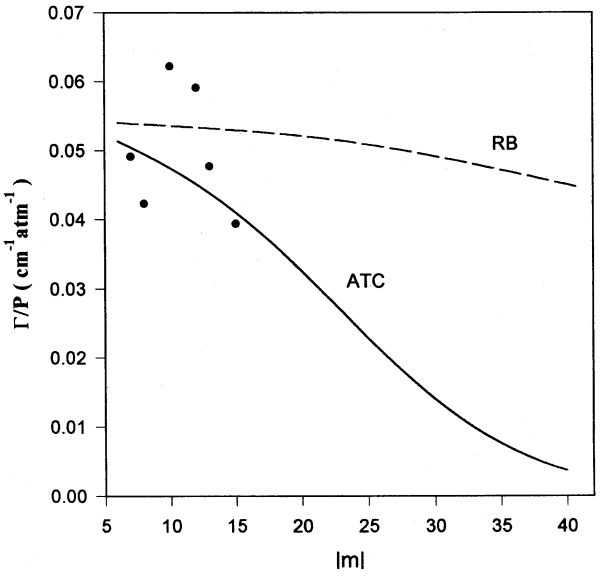

Fig. 3. Plot of calculated Γ/P values against $|m|$. The observed values are also shown symbolically, m being $-J_{\rm i}$ for P-branch and $J_{\rm i}+1$ for R-branch.

rotational states of the absorber. This is in agreement with the change of γ values for the small range of J values investigated in the present work. The non-resonant contribution from inelastic collision for a fixed transition of the absorber is small in the interruption probability function $S_2\,(b,\bar{v})$ because of the absence of J-states of the perturber. The re-orientation effect [35] is significant during the collision induced transitions rather than rotational phase shifts of the active molecule. Nearly 90% contribution to the J-dependence of the half width values will arise from the first part of equation (9).

The calculation of pressure broadening coefficients is also performed using the RB-model based on classical path assumption. The inelastic collision probability function $S(b,v)$ in equation (6) includes no effect of the term diagonal in the rotational states of the spherical perturber helium. According to RB-model, neglecting the vibrational phase-shift the equation (9) can be written as,

$$\int_0^\infty S(b,\bar{v})\,2\pi b\,{\rm d}b = \int_0^\infty \left[1-\exp(-S_2(b,\bar{v}))\right]\,2\pi b\,{\rm d}b. \quad (10)$$

The above equation avoids the cutoff procedure required in the ATC-model. A simple numerical integration technique has been employed to calculate the values of broadening coefficients (shown in Tab. 1) this was done by increasing the value of the impact parameter, b with a step size of 0.001 Å up to the limit of convergence. The calculated values in RB-model are in good agreement with the observed values for R-branch transitions rather than for P-branch transitions and are not able to show strong J-dependence with increasing J values of the absorber (Fig. 3). The halfwidth values are somewhat overestimated when calculated by the RB-model unlike those that obtained from the ATC-model.

Due to a correlation term between contributions from long range and short range parts of the TH-potential in the expression of $S_2(b,\bar{v})$ in equation (7), it is not possible to conclude about the relative contribution for the two parts of the potential to the values of halfwidths by applying either the ATC- or RB-model. In this situation, the adiabatic collisional phase-shift can be taken into account to describe the above phenomenon to some extent. The term collisional phase-shift may arise from the interruption of radiation emitted or absorbed, caused by collision of emitter or absorber with the perturbers. If two resonating energy levels are perturbed by collision the resonating energy can be written as,

$$\Delta E = (E_{\rm f}-E_{\rm i}) + (\Delta E_{\rm f}-\Delta E_{\rm i}). \quad (11)$$

The phase-shift, η corresponds to the difference between the perturbed energies in the above equation. In binary collision approach it depends on the angular shift in the internuclear distance between two colliders, having specific orientations, relating to one optical transition. For one rovibronic transition, each of $\Delta E_{\rm f}$ and $\Delta E_{\rm i}$ is determined by the first order perturbation of the interaction Hamiltonian averaged over all possible orientations of the colliders in their specified states [28]. Here it is to be noted that only the isotropic part of the interaction potential contributes to the phase-shift and no quantum number dependence is observed. However, the dependence of phase-shift on the impact parameter and the relative contribution of the interaction potentials can be discussed quite satisfactorily. In general, the interaction potential of the form C/R^n will yield the phase-shift [35,36],

$$\eta = \frac{2\pi}{h}\int_{-\infty}^{+\infty}\frac{C_{\rm f}-C_{\rm i}}{R^n}\,{\rm d}t \quad (12)$$

where we assume a straight path trajectory model for relative approach of two colliders $R(t)=\sqrt{\bar{v}^2\,t^2+b^2}$ and $C_{\rm f}$, $C_{\rm i}$ the potential parameters for final and initial states of one rovibrational transition respectively. In our spectroscopic limit the values of potential parameters in the upper vibrational state are not known. The following technique will be useful to perform the above integration in such cases. The first term of equation (3) represents the isotropic part of the TH-potential to be used in the evaluation of η. The vibrational dependence of attractive well depth ϵ of the intermolecular potential (Eq. (3)) does not depend strongly on the vibrational excitation of the absorber molecule. So, the change in the constant C (Eq. (12)), upon vibrational excitation, arises mainly from the change in the impact parameter σ which depends on the molecular diameter for both the excited and the ground states of the colliding molecules (Eq. (5)) in the potential $V_{\rm TH}(R)$. According to equation (12) we can get,

$$\eta = \frac{8\pi\epsilon}{h}\int_{-\infty}^{+\infty}\left[\frac{(\sigma_{\rm f}^6+\sigma_{\rm i}^6)(\sigma_{\rm f}^6-\sigma_{\rm i}^6)}{R^{12}}-\frac{(\sigma_{\rm f}^6-\sigma_{\rm i}^6)}{R^6}\right]{\rm d}t. \quad (13)$$

Considering the weak interaction process involved in fourth order combination-overtone band transition of acetylene, we can neglect the small vibrational dependence of σ. Then the above equation simplifies into the following form, if $\sigma_{\rm f}$ is close to $\sigma_{\rm i}$,

$$\eta = \frac{8\pi\epsilon(\sigma_{\rm f}^6 - \sigma_{\rm i}^6)}{h} \left[\int_{-\infty}^{+\infty} \frac{2\sigma_{\rm i}^6}{R^{12}}\,{\rm d}t - \int_{-\infty}^{+\infty} \frac{1}{R^6}\,{\rm d}t\right]. \quad (14)$$

After integration with $R(t) = \sqrt{\bar{v}^2\,t^2 + b^2}$ we get,

$$\eta = \frac{8\pi\epsilon\sigma_{\rm i}}{h\bar{v}} \left[\left(\frac{\sigma_{\rm f}}{\sigma_{\rm i}}\right)^6 - 1\right] f(b)$$

where,

$$f(b) = \frac{3\pi}{8}\left(\frac{\sigma_{\rm i}}{b}\right)^5 \left[\frac{21}{16}\left(\frac{\sigma_{\rm i}}{b}\right)^6 - 1\right]. \quad (15)$$

The function $f(b)$ contains the explicit impact parameter dependence of the contributions from repulsive and attractive parts of the TH-potential into phase-shift. So, we can estimate the relative importance of repulsive and attractive parts of the TH-potential for close collision interaction phenomena. For the closest approach $d = 2.93$ Å, used in the ATC-model, the ratio of the contributions from the repulsive and the attractive parts of the potential is 4:1. Hence the attractive part of the potential will have only 31.3% contribution at cutoff value. In Figure 4, the variation of $f(b)$ over small values of the impact parameter shows explicit dependence of the contributions from the two parts of the TH-potential. For small b values, the repulsive part dominates over the attractive part. For $b = 3.72$ Å, the contributions from two different parts of the potential cancel each other, $f(b)$ becomes zero resulting in null phase-shift. For higher values of b, the attractive part is larger but both of them tend to zero, so that $f(b)$ approaches zero. For close proximity of $\sigma_{\rm f}$ to $\sigma_{\rm i}$, the magnitude of phase-shift will be very small.

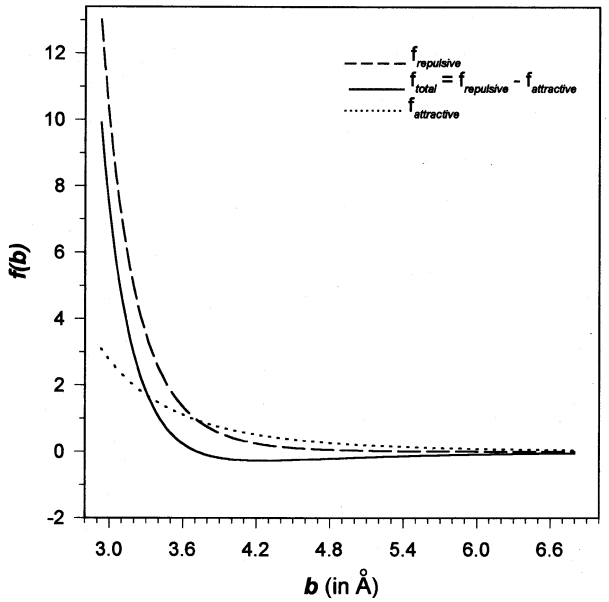

Fig. 4. Plot of $f(b)$ exhibiting the impact parameter (b) dependence of repulsive part ($f_{\rm repulsive}$), attractive part ($f_{\rm attractive}$) and joint repulsive and attractive parts ($f_{\rm total}$) of the TH-potential discussed in the text.

5 Conclusions

The wavelength modulation technique has been adopted for high resolution near the IR diode laser spectroscopic measurement of helium broadened absorption lines of the acetylene ($\nu_1 + 3\nu_3$) band transitions. To our knowledge He-broadening measurements of this near infrared band have not been published so far except for only one transition R15 [5]. The modulation parameters are chosen carefully to obtain a distortion free line shape. The pressure broadening coefficients (HWHM) and linestrength parameters of six rotational components are obtained by simulation and fitting with the standard Voigt profiles. The residuals could not be improved by collisionally narrowed line shape function. Small asymmetry in the wings could arise from high pressure used in the work. This could not be explained by theoretical simulation. Previous infrared measurements of acetylene rovibrational transitions in the presence of perturber gases, for the (ν_5) band transitions in references [33,37], ($\nu_4 + \nu_5$) band transitions in references [38,39] and for the ($\nu_1 + 3\nu_3$) band and other combination-overtone band transitions in references [3,5, 40], did not show any evidence of narrowing. In references [38–40], the measurements were performed mainly to describe the molecular parameters in the respective band transitions along with the line assignments. The pressure broadening coefficients obtained for the six transitions are comparable to those of the other rotational transitions measured by Lucchesini *et al.* [5] who reported the FWHM values. Specifically, for He-broadened R15 transition, the HWHM value of the broadening coefficient, 3.7 MHz/torr (≈ 0.0937 cm^{-1}atm^{-1}) in reference [5], is of the same order in magnitude as our observed values. The values of observed helium broadening coefficients are reasonable if compared with the values of air broadening coefficients of ν_5 band transitions in reference [37] and ($\nu_1 + 3\nu_3$) band transitions in reference [7]. Typically for P7 transition, the value of air broadening coefficient

$$\frac{\Gamma}{P}({\rm air}) = 0.79\frac{\Gamma}{P}({\rm N_2}) + 0.21\frac{\Gamma}{P}({\rm O_2})$$

for a fundamental band in reference [37] is 42% greater while for a combination overtone band in reference [7] it is 37% greater than the value of helium broadening coefficient in this measurement. The theoretical calculations of the broadening coefficients are also carried out under semi-classical impact theories on the basis of ATC- and RB-model. In this work we prefer to use the ATC-model to describe the quantum number dependence of pressure broadening coefficients rather than the RB-model in the range of $|m|$-values (Fig. 3) investigated. The agreement of the self-, N_2-, O_2- and air-broadening coefficients,

calculated by the ATC-model with the observed data for different rotational components, was also found to be satisfactory [7]. The calculation of self-, air- and noble-gas broadening coefficients of benzene in reference [41] show the success of ATC theory to describe the quantum number dependence of the broadening coefficients with sufficient accuracy. The relative dependence of two radial parts in the TH-potential on close collisional dephasing is discussed in a simple way. The calculation shows the importance of the isotropic potential used in this trajectory model. The better results for the value of γ have been obtained by using TH potential having two adjustable parameters A_2 and R_2. $A_2 = R_2 = 0.40$ is the suitable value obtained for TH parameters in our spectroscopic limit. The agreement of calculated and observed values is very good for the P-branch transitions. As J increases the calculated half width values go on decreasing up to the order of 0.01 $cm^{-1}atm^{-1}$ till $J = 35$. This is due to very small population of the active molecule for higher J's, so that interaction with the perturber is sufficiently small. The irregular rotational dependence of the observed values may arise from vibrational perturbation and is beyond our theoretical estimation. It should be noted that the range of our observed J-values is also small. The calculated changes of the phase-shift with the impact parameter have been evaluated using the classical trajectory model. This shows the dominance of the repulsive part of the potential for low values of impact parameter. Collisions with fast ions having small impact parameter have been studied in atomic physics [42–44]. However, there are no direct measurements on atom-molecule collisions at low energies.

D.B. and B.R. thank the Council of Scientific and Industrial Research, New Delhi for Senior Research Fellowships (Extended). Financial assistances from the Department of Science and Technology (SP/S2/L–05/96) are gratefully acknowledged.

References

1. K. Hedfeld, P. Lueg, Z. Phys. **77**, 446 (1932).
2. B.C. Smith, J.S. Winn, J. Chem. Phys. **94**, 4120 (1991).
3. F.S. Pavone, F. Marin, M. Inguscio, K. Ernst, G. Di Lonardo, Appl. Opt. **32**, 259 (1993).
4. X. Zhan, H. Halonen, J. Mol. Spectrosc. **160**, 464 (1993).
5. A. Lucchesini, M. De Rosa, D. Pelliccia, A. Ciucci, C. Gabbanini, S. Gozzini, Appl. Phys. B **63**, 277 (1996).
6. D. Biswas, B. Ray, S. Dutta, P.N. Ghosh, Appl. Phys. B **68**, 1125 (1999).
7. B.K. Dutta, D. Biswas, B. Ray, P.N. Ghosh, Eur. Phys. J. D **11**, 99 (2000).
8. J. Waschull, F. Kühnemann, B. Sumpf, J. Mol. Spectrosc. **165**, 150 (1994).
9. V.V. Pustogov, F. Kühnemann, B. Sumpf, Y. Heiner, Ka. Herrmann, J. Mol. Spectrosc. **167**, 288 (1994).
10. B. Sumpf, O. Fleischmann, J. Waschull, Y. Heiner, H.-D. Kronfeldt, Infrared Phys. Technol. **36**, 439 (1995).
11. V.V. Lazarev, Yu.N. Ponomarev, B. Sumpf, O. Fleischmann, J. Waschull, H.-D. Kronfeldt, V.N. Stroinova, J. Mol. Spectrosc. **173**, 177 (1995).
12. D. Biswas, B. Ray, P.N. Ghosh, Chem. Phys. Lett. **275**, 314 (1997).
13. A.S. Pine, J. Mol. Spectrosc. **82**, 435 (1980).
14. D.R. Rao, T. Oka, J. Mol. Spectrosc. **122**, 16 (1987).
15. P.W. Anderson, Phys. Rev. **76**, 647 (1949).
16. C.J. Tsao, B. Curnutte, J. Quant. Spectrosc. Radiat. Transfer **2**, 41 (1962).
17. D. Robert, J. Bonamy, J. Phys. **40**, 923 (1979).
18. B. Ray, P.N. Ghosh, Spectrochim. Acta A **53**, 537 (1997).
19. A.K. Hui, B.H. Armstrong, A.A. Wray, J. Quant. Spectrosc. Radiat. Transfer **19**, 509 (1977).
20. P.R. Bevington, *Data Reduction and Error Analysis for the Physical Sciences*, 1st edn. (McGraw-Hill, New York, 1969).
21. W.H. Press, S.A. Teukolsky, W.T. Vetterling, B.P. Flannery, *Numerical Recipes in FORTRAN. The art of Scientific Computing*, 2nd edn. (Cambridge University Press, Cambridge, 1992).
22. J.P. Bouanich, G. Blanquet, J.C. Populaire, J. Walrand, J. Mol. Spectrosc. **190**, 7 (1998).
23. L. Galatry, Phys. Rev. **122**, 1218 (1961).
24. A.S. Pine, J. Chem. Phys. **101**, 3444 (1994).
25. R.H. Tipping, R.M. Herman, J. Quant. Spectrosc. Radiat. Transfer **10**, 881 (1970).
26. G.C. Maitland, M. Rigby, E.B. Smith, W.A. Wakeham, *Intermolecular forces – their origin and determination*, 1st edn. (Oxford University Press, New York, 1981).
27. L.C. Biedenharn, J.M. Blatt, M.E. Rose, Rev. Mod. Phys. **24**, 249 (1952).
28. A. Ben-Reuven, S. Kimel, M.A. Hirschfeld, J.H. Jaffe, J. Chem. Phys. **35**, 955 (1961).
29. M. Giraud, D. Robert, L. Galatry, J. Chem. Phys. **53**, 352 (1970).
30. *CRC Handbook of Chemistry and Physics*, edited by R.C. Weast, 58th edn. (CRC Press, Florida, 1977–78).
31. J.O. Hirschfelder, C.I. Curtiss, R.B. Bird, *Molecular Theory of Gases and Liquids*, 1st edn. (Wiley, New York, 1954).
32. G. Herzberg, *Infrared and Raman Spectra of Polyatomic Molecules*, 1st edn. (Van Nostrand, New York, 1945).
33. J.P. Bouanich, D. Lambot, G. Blanquet, J. Walrand, J. Mol. Spectrosc. **140**, 195 (1990).
34. L.W. Bruch, I.J. McGee, J. Chem. Phys. **46**, 2959 (1967).
35. R.G. Gordon, J. Chem. Phys. **44**, 3083 (1966).
36. M.H. El Ghajaly, A.M. Abd El Baky, A.F. Mansour, A.H. Bassyouni, J. Quant. Spectrosc. Radiat. Transfer **61**, 729 (1999).
37. D. Lambot, G. Blanquet, J.P. Bouanich, J. Mol. Spectrosc. **136**, 86 (1989).
38. P. Varanasi, L.P. Giver, F.P.J. Valero, J. Quant. Spectrosc. Radiat. Transfer **30**, 497 (1983).
39. P. Varanasi, L.P. Giver, F.P.J. Valero, J. Quant. Spectrosc. Radiat. Transfer **30**, 505 (1983).
40. Y. Ohsugi, N. Ohashi, J. Mol. Spectrosc. **131**, 215 (1988).
41. J. Waschull, Y. Heiver, B. Sumpf, H.D. Kronfeldt, J. Mol. Spectrosc. **190**, 140 (1998).
42. E. Everhart, Q.C. Kessel, Phys. Rev. Lett. **14**, 247 (1995).
43. Q.C. Kessel, E. Everhart, Phys. Rev. A **16**, 146 (1996).
44. R. Döerner, V. Mergel, O. Jagutzki, L. Spielberger, U. Ullrich, R. Moshammer, H. Schmidt-Böcking, Phys. Rep. **330**, 95 (2000).